We are IntechOpen, the world's leading publisher of Open Access books Built by scientists, for scientists

6,900
Open access books available

185,000
International authors and editors

200M
Downloads

Our authors are among the

154
Countries delivered to

TOP 1%
most cited scientists

12.2%
Contributors from top 500 universities



WEB OF SCIENCE™

Selection of our books indexed in the Book Citation Index in Web of Science™ Core Collection (BKCI)

Interested in publishing with us?
Contact book.department@intechopen.com

Numbers displayed above are based on latest data collected.
For more information visit www.intechopen.com



Chapter

Nonlinear Dynamical Regimes and Control of Turbulence through the Complex Ginzburg-Landau Equation

Joël Bruno Gonpe Tafo, Laurent Nana, Conrad Bertrand Tabi and Timoléon Crépin Kofané

Abstract

The dynamical behavior of pulse and traveling hole in a one-dimensional system depending on the boundary conditions, obeying the complex Ginzburg-Landau (CGL) equation, is studied numerically using parameters near a subcritical bifurcation. In a spatially extended system, the criterion of Benjamin-Feir-Newell (BFN) instability near the weakly inverted bifurcation is established, and many types of regimes such as laminar regime, spatiotemporal regime, defect turbulence regimes, and so on are observed. In finite system by using the homogeneous boundary conditions, two types of regimes are detected mainly the convective and the absolute instability. The convectively unstable regime appears below the threshold of the parameter control, and beyond, the absolute regime is observed. Controlling such regimes remains a great challenge; many methods such as the nonlinear diffusion parameter control are used. The unstable traveling hole in the one-dimensional cubic-quintic CGL equation may be effectively stabilized in the chaotic regime. In order to stabilize defect turbulence regimes, we use the global time-delay auto-synchronization control; we also use another method of control which consists in modifying the nonlinear diffusion term. Finally, we control the unstable regimes by adding the nonlinear gradient term to the system. We then notice that the chaotic system becomes stable under strong nonlinearity.

Keywords: Benjamin-Feir-Newell instability, subcritical bifurcation, complex Ginzburg-Landau equation, unstable traveling hole

1. Introduction

Many complex systems evolve in a non-equilibrium environment. Further out of the equilibrium [1], these systems tend to display progressively more complicated dynamics. The non-chaotic patterned state and spatiotemporal chaos are observed in the system. In the domain of the envelope equations, the quintic complex Ginzburg-Landau (CGL) equation is appropriate to obtain stable localized solutions (pulses, holes) [1, 2]. Among physical applications of the quintic CGL equation, one

IntechOpen

can mention binary fluid convection [3], spiral waves in the Couette-Taylor flow between counterrotating cylinders [4], wave propagation in nonlinear optical fibers with gain and spectral filtering [5], the oscillatory chemical reaction [6], hydrodynamic turbulence [7], chemical turbulence [8, 9], and electrical turbulence in the cardiac muscle [10]. Our work focuses on two types of systems: the spatially extended system and the finite system. In the case of spatially extended systems, we use as initial conditions a traveling-hole solution with periodic boundary conditions [11–15]. All the dynamical regimes obtained during our work are summarized in a phase diagram. In the case of the finite domain, we use as initial condition a pulse solution. Wave patterns are described by CGL equation in which the amplitude of the wave pattern vanishes at the lateral boundaries of the domain in order to retrieve numerically some coherent structures observed experimentally, in the case of absolute or convective instabilities [16–18].

Over the past decade, problems of chaos control and synchronization started to play a central role in the studies of chaotic dynamics [19] in many different areas such as chemistry [20], laser physics [21], electronic circuits [22], plasma [23], and mechanical systems. Since the pioneering work of Ott et al. [24] on the control of low-dimensional chaos in nonlinear systems based on Floquet theory, chaos control techniques have been well developed [25, 26]. Up to date, many control techniques have been suggested to control low-dimensional chaos by stabilizing unstable periodic orbits or fixed points. The realization of chaos control mainly includes feedback and non-feedback methods, both of which have advantages and disadvantages. Pyragas is one of the first to work on a delayed feedback loop called time-delay auto-synchronization (TDAS) [25]. Another part of our works is to control turbulence regimes observed, in particular the defect turbulence regime by employing the methods already successfully used in the cubic case, namely, the nonlinear diffusion technique [20], the feedback method [27], and the lower-order complex Ginzburg-Landau (LOCGL) equation [28–31]. The LOCGL equation which describes a system exhibiting a subcritical bifurcation to traveling waves must contain a quintic nonlinearity. It is obtained by adding nonlinear terms to the system. The effects of the nonlinear gradient terms are confirmed by using some indicators such as the Lyapunov exponent and the energy bifurcation diagram. Most of the results related to these different aspects are presented in the rest of this work.

2. Dynamics of traveling hole in one-dimensional systems near subcritical bifurcation

2.1 Model description

We consider a subcritical Hopf bifurcation, with a one-dimensional complex amplitude $A(x,t)$ and complex coefficients given by

$$\frac{\partial A}{\partial t} = (1+ic_1)\frac{\partial^2 A}{\partial x^2} + \mu A + (1-ic_3)|A|^2 A - (1-ic_5)|A|^4 A, \tag{1}$$

where c_1, c_3, c_5, and μ are real constants. μ is the parameter control, and t and x represent, respectively, temporal and spatial variables. This equation is a paradigmatic model for the study of spatiotemporal dynamics [11]. It admits many different types of stable pulses [32] and hole-like [17] solutions. We have imposed on the complex amplitude the following boundary conditions: We consider a system in which we impose periodic boundary conditions:

$$A(x,t) = A(x+L,t), \tag{2}$$

where L is the length of the domain. These boundary conditions are realized in different extended systems, where the pattern amplitude vanishes near lateral boundaries. We have chosen as initial condition a hole solution given by [15]:

$$A(x,0) = \exp\left(i\left[q_{ex}x + (\pi/2)\tanh(\gamma x)\right]\right). \tag{3}$$

The precise form of the initial condition is not important here as long as we have a one-parameter family of localized phase-gradient peaks. This is because the left moving and right moving coherent holes for fixed c_1, c_1, and q_{ex} are each unique and have one unstable mode only. As γ is varied, three possibilities can arise for the time evolution of the initial peak: evolution toward a defect. The nonzero q_{ex} breaks the left-right symmetry and results in the differing periods of the left and right moving edge holes [15].

2.2 Results of numerical simulation

The parameters $c_{3,}$, γ, and q_{ex} were fixed at c_3 = 0.50, $\mu = 1$, $\gamma = 1.0$, and $q_{ex} = -0.03$. And, we have varied c_1 and c_5. This variation enabled us to identify, in the parameter space (c_1, c_5), zones in which the patterns exhibit different behaviors. The different asymptotic phases observed are summarized in the state diagram of **Figure 1**, where the solid line corresponds to analytical results and represents the BFN line, while dashed lines are numerical ones. Dashed lines are obtained by varying c_1 and c_5 which gave us regions of different regimes. We have identified plane waves, spatiotemporal intermittency, phase turbulence, and weak turbulence and defect turbulence regimes.

2.2.1 Plane wave regime

The plane wave regime is a laminar state where no chaos is observed. The plane wave is localized below the BFN line in a zone called stable zone. The spatial profile

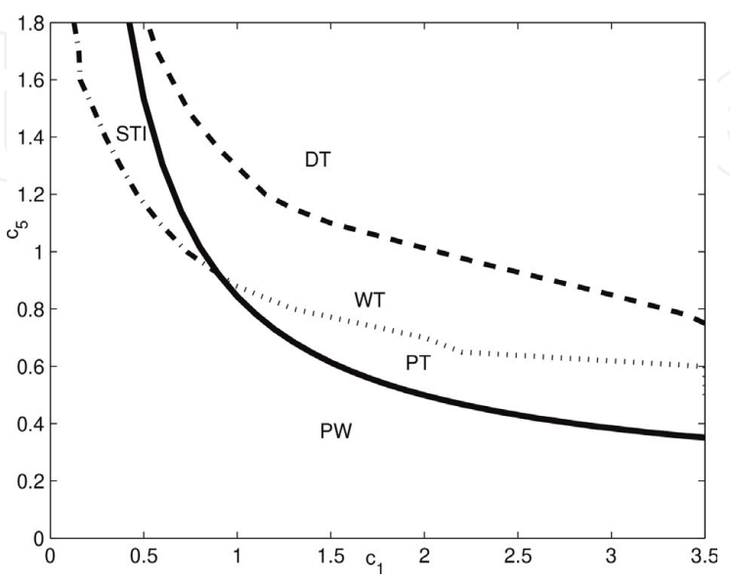


Figure 1.
Phase diagram of an initial traveling hole of the quintic CGLE showing different types of dynamical regimes: plane wave (PW), spatiotemporal intermittency (STI), phase turbulence (PT), weak turbulence (WT), defect turbulence (DT). $c_3 = 0.5$, and $\mu = 1.0$.

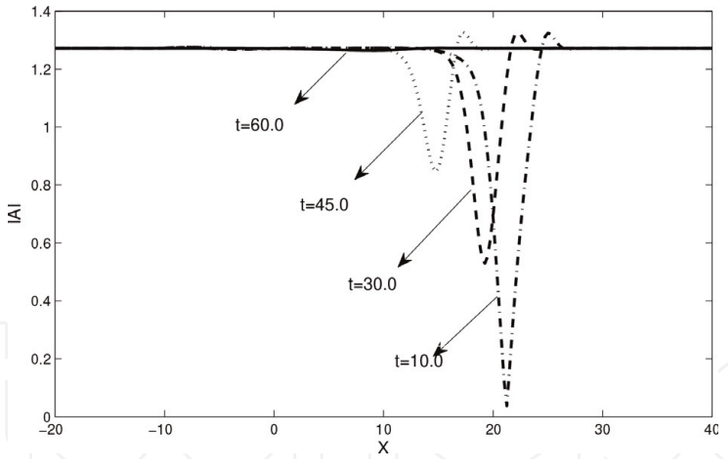


Figure 2.
Space-time plot of the wave amplitude |A| in the case of the Benjamin-Feir stability for $c_1 = 2.5$, $c_3 = 2.0$, and $c_5 = 0.4$.

of the wave patterns in the plane wave regime is shown in **Figure 2**. We notice that by the growing of the time, the regime still stable, and laminar regime is observed.

2.2.2 Spatiotemporal intermittency regime

It consists of space-time regions of stable plane waves separated by localized objects evolving and interacting in a complex manner [33]. It represents a special scenario of transition to turbulence in extended systems: it is characterized by the coexistence of laminar (ordered) and turbulent (disordered) domains that occur randomly in different places of the system for the same values of the control parameters [13, 33]. It has been observed in many experiments such as plane Couette flow, counterrotating Taylor-Couette flow, and Taylor-Dean system. In 1D extended systems, spatiotemporal intermittency has been observed in rectangular and annular Rayleigh-Bénard cells at large values of the Rayleigh number [15]. This spatiotemporal intermittency occurs via a subcritical bifurcation from purely laminar state, and the coexistence of two different stable states can be described phenomenologically using an amplitude equation derived from a Lyapunov function. We have plotted in **Figure 3** the characteristic pattern of a spatiotemporal intermittency in which a global mode coexists with a chaotic attractor: the state consists of patches of plane waves, which are separated y various holes. **Figure 3b** and **c** shows in detail how a hole generates a phase defect and in turn generates two daughter holes close-up of the amplitude $|A|$ and close-up of the complex phase.

2.2.3 Phase turbulence regime

Just above the BFN line, the phase turbulence regime is observed (**Figure 4**). It is best defined by the absence of space-time defects. In this regime, the region is a weakly disordered one in which $|A(x,t)|$ remains away from zero. The absence of phase singularities implies that the "*localwavenumber*" given by

$$\nu = \frac{1}{L}\int_0^L dx \partial_x \Psi(x,t), \tag{4}$$

where $\Psi(x,t)$ is the phase, is a conserved quantity. A global wave number of the configuration can be defined as $k \equiv 2\pi/L$. Chaos is very weak (see **Figure 4**). So the global phase difference becomes the constant of the motion and is conserved. This is corroborated by the flat shoulder of the spatial power spectrum of $|A(x,t)|$ at low

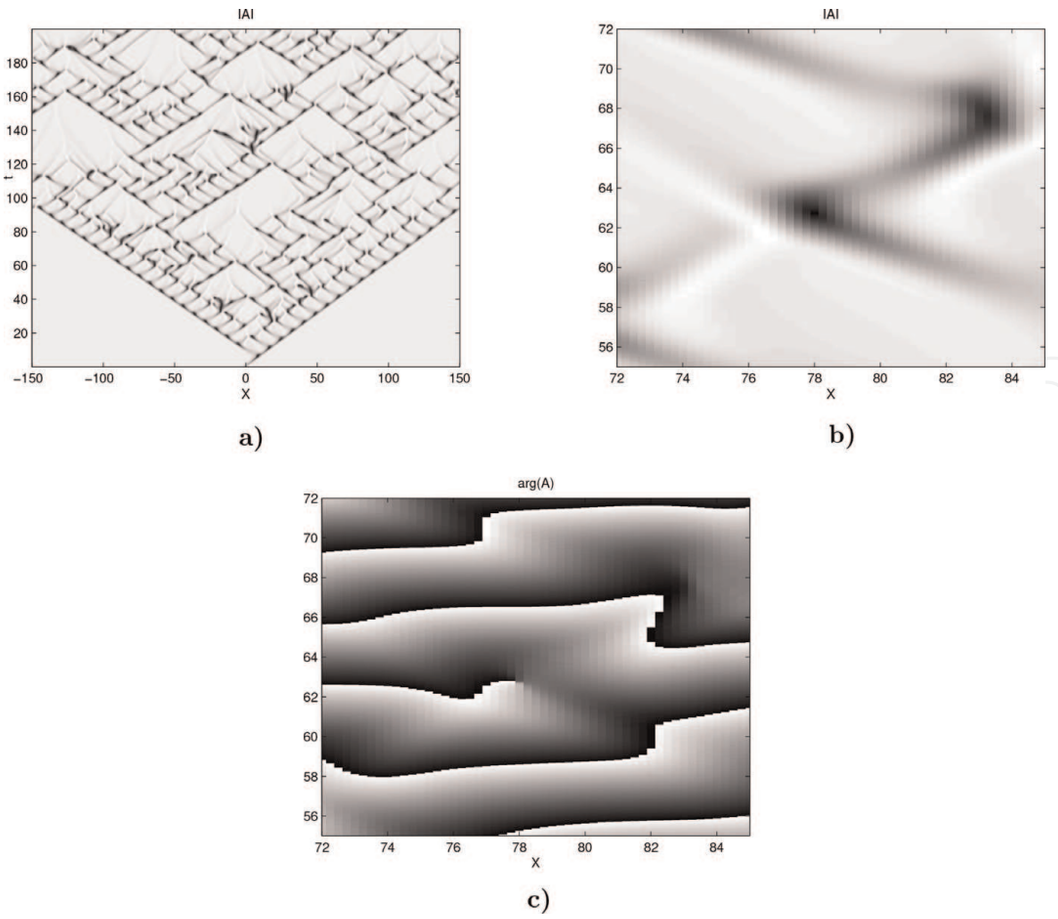


Figure 3.
Space-time gray-scale plots showing the invasion of a plane wave state by hole-defect chaos: (a) wave amplitude, |A| (dark: |A| ≈ 0), and (b) close-up of $c_3 = 0.5$; $c_5 = 1.1$ showing in detail how a hole generates a phase defect that, in turn, generates two daughter holes: $c_1 = 0.59$, $c_3 = 0.5$, $c_5 = 1.1$.

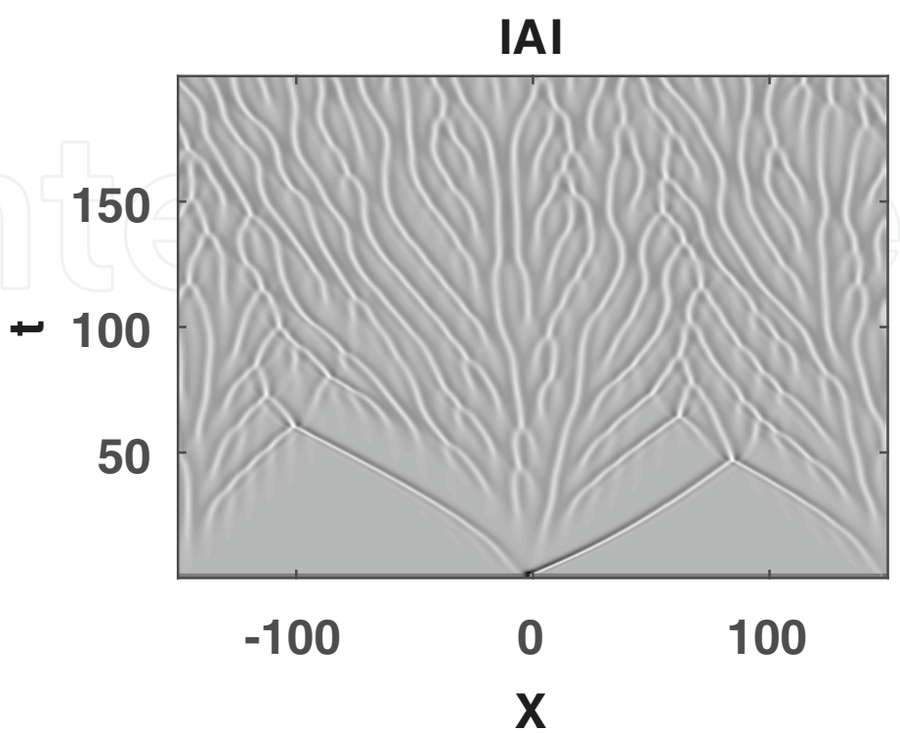


Figure 4.
Phase turbulence regime of |A|, for $c_1 = 1.5$, $c_3 = 0.5$, and $c_5 = 0.5$.

wavenumbers, reminiscent of the Kuramoto-Sivashinsky equation (KS). The dynamics is in fact very similar to that of KS, which is not surprising since this equation was originally derived to describe the phase dynamics of CGL equation near the BFN line.

2.2.4 Weak turbulence regime

Beyond the BFN line, we observe that for the parameter equations (c_1, c_5) larger, a weak turbulence regime is observed [2] (see **Figure 5**). Weak turbulence theory was developed in the 1960s to provide equations which quantitatively describe the transfer of energy among turbulent, weakly nonlinear, and dispersive waves in fluids [34]. The basic or kinetic equations produced by weak turbulence theory have been applied to analyze energy transfer including internal and surface waves with small aspect ratios in the atmosphere and ocean [35]. They are also observed in the case of two spatial dimensions [3, 36]. As we observe in **Figure 5**, holes move across the system (darker lines in **Figure 5**), while the amplitude of wave patterns at their cores changes. A black region along a gray line indicates amplitude $|A|$ near zero at the core of the hole. Each hole may spawn new holes, which in turn contribute to the loss of spatial coherence of the solution. **Figure 6** shows the evolution of one hole of **Figure 5** from its creation to its disappearance.

2.2.5 Defect turbulence

Father away from the BFN line a spatiotemporally disordered regime called amplitude or defect turbulence is observed (see **Figure 7**). The behavior in this region is characterized by defects. The defect turbulence regime is the dynamical regime wherein the fluctuations of $|A|$ become dominant over the phase dynamics.

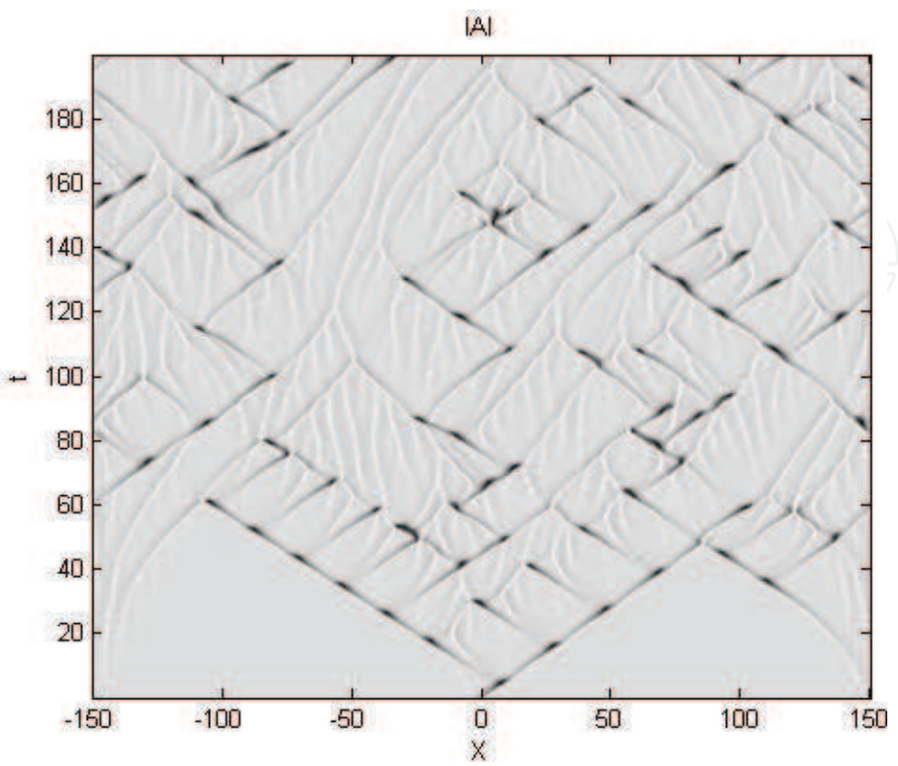


Figure 5.
Weak turbulence regime observed for $c_1 = 1.5$, $c_3 = 0.5$, and $c_5 = 0.9$.

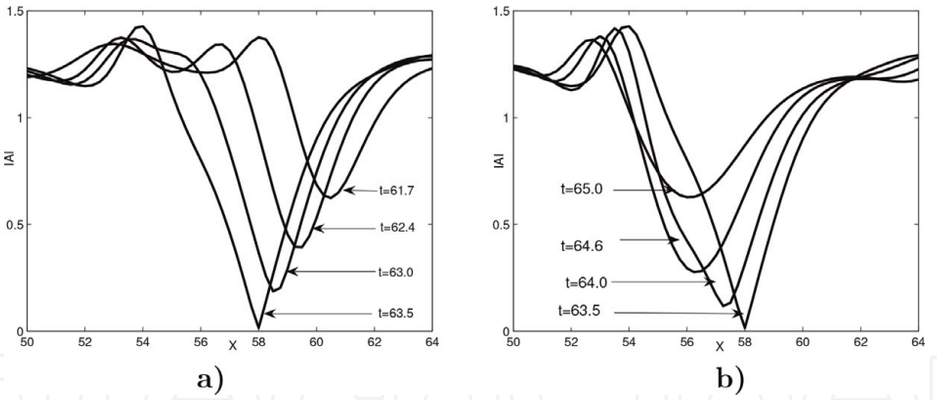


Figure 6.
(a) Formation and (b) disappearance of a hole between $t = 61.5$ and $t = 64.5$ in the numerical simulation of ***Figure 5****.*

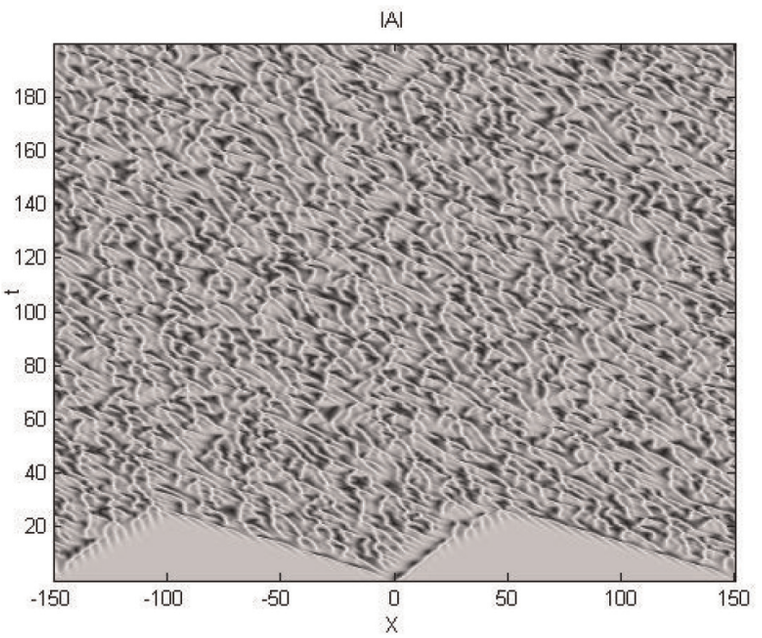


Figure 7.
Defect turbulence regime observed for $|A|$, with $c_1 = 2.5$, $c_3 = 0.5$, $c_5 = 1.1$.

The complex field experiences therefore large amplitude oscillations which can (locally and occasionally) cause $|A|$ to vanish. As a consequence, at all those points (hereinafter called space-time defects or phase singularities), the global phase of the field $\Phi \equiv \arctan\left[\frac{\mathrm{Im}(A)}{\mathrm{Re}(A)}\right]$ shows a singularity.

3. Nonlinear structures of traveling waves in subcritical systems with finite geometries

3.1 The cubic-quintic complex Ginzburg-Landau equation in a finite domain

The one-dimensional cubic-quintic CGL equation in this case is given by:

$$\frac{\partial A}{\partial t} = \nu \frac{\partial A}{\partial x} + (1 + ic_1)\frac{\partial^2 A}{\partial x^2} + \mu A + (1 - ic_3)|A|^2 A - (1 - ic_5)|A|^4 A, \qquad 0 \le x \le L. \tag{5}$$

This equation describes the envelope of a traveling wave propagating at the group velocity v toward negative x [18]. L is the length of the domain. This model equation arises in physics as an amplitude equation, providing a reduced universal description of weak nonlinear spatiotemporal phenomena in extended continuous media in the proximity of a subcritical Hopf bifurcation. The homogeneous boundary conditions are given by:

$$A(x = 0, t) = A(x = L, t) = 0. \tag{6}$$

Figure 8 illustrates the deterministic evolution of wave pattern amplitude for convective instability and absolute instability regimes. In the case of convective regime, the wave patterns disappear with the time, while in the case of the absolute instability, they propagate in the whole system.

3.2 Stability of wave patterns of the 1D cubic-quintic CGLE

Let us note that, in the convective regime, the localized disturbances of the basic state are growing but step away from the source. This is why we have restricted the study to the dynamics of pattern for parameters corresponding to the absolute instability regime. When the criticality parameter μ increases, the linear stability fails, and the waves can involve into new localized structures. The periodic basic solution loses its stability, a secondary instability appears, and we can observe new states in the domain (see **Figure 9**) [18, 37]. As we can see in **Figure 9**, for a value the control parameter μ greater than a critical value μ_c, secondary structures will appear at the left boundary of the system and destabilize the system [4, 18]. These secondary structures create spatiotemporal chaos regime (regimes with defect, holes, etc.) into the system.

3.3 Numerical simulations of the 1D cubic-quintic CGLE

We investigate the effects of the quintic nonlinear dispersion coefficient c_5 in Eq. (5) with the homogeneous boundary conditions. The simulation was started

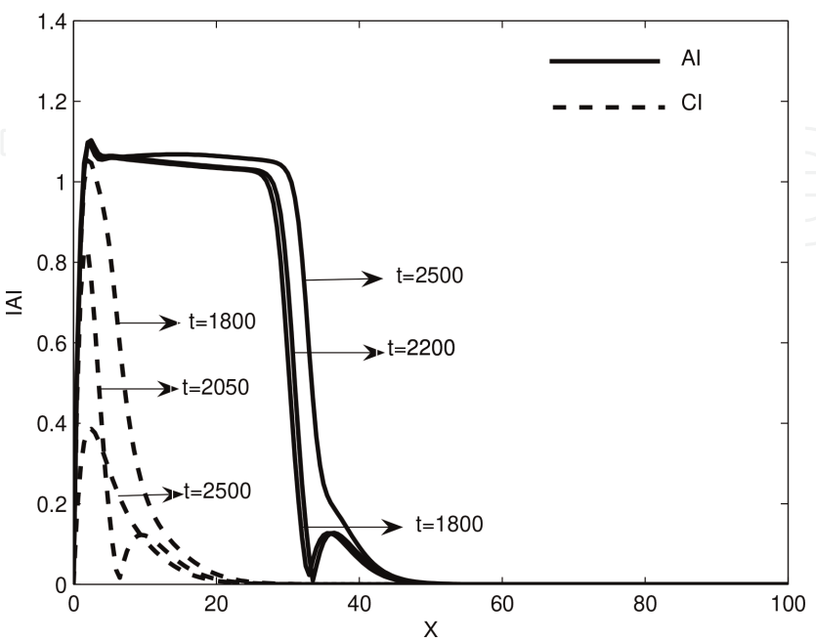


Figure 8.
Profiles of the amplitude of an initial perturbation at different times for $v = 1.0$, $c_1 = 0.45$, $c_3 = 2.0$, $c_5 = 2.0$, and $L = 100$: in the convective instability (CI) regime with $\mu = 0.15$ (dashed lines) and in the absolute instability (AI) regime with $\mu = 0.3$ (solid lines).

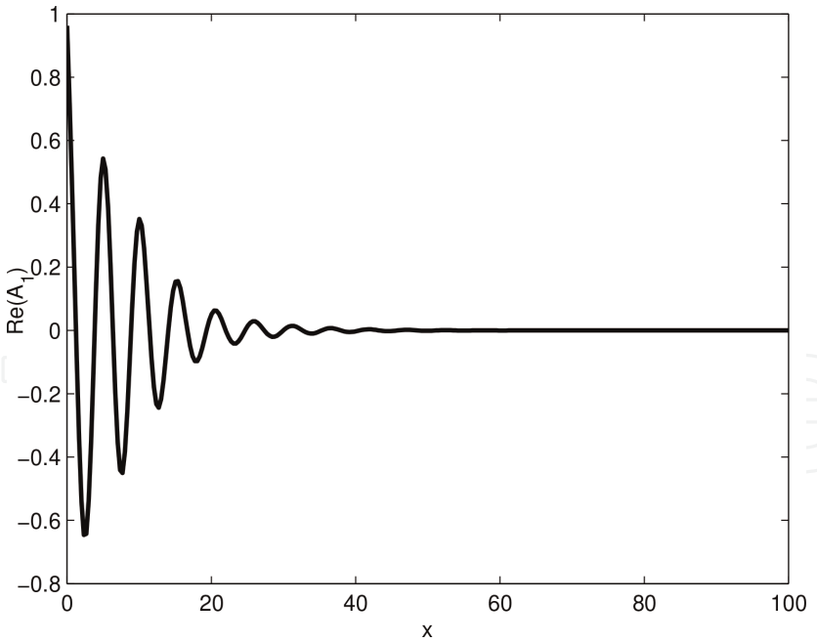


Figure 9.
Graph of $Re(A_1)$ for $c_1 = 0.45$, $c_3 = 2.0$, $c_5 = 2.0$, $L = 100$, $\mu = 1.4$, $\Omega = 1.2$, and $v = 1.0$.

from an approximation of a pulse-like solution with a low amplitude. We investigate the effects of the quintic nonlinear coefficient c_5 with the homogeneous Dirichlet boundary conditions. Solving the 1D cubic-quintic CGLE for several values of c_5 in the absolute instability regime leads to bifurcation of the global mode to new states that are summarized in the phase diagram of **Figure 10** for c_5 and ε [−1.5;3.5]. We have found that the threshold of convective-absolute instability is μ_α = 0.207. Our phase diagram is obtained only in the absolute instability regime ($\mu > \mu_\alpha$). For the positive values of c_5, global mode regime and chaotic regimes are observed; they are separated by the line L_1. The global mode is a stable regime. The secondary structures are created by the secondary front which is close to the

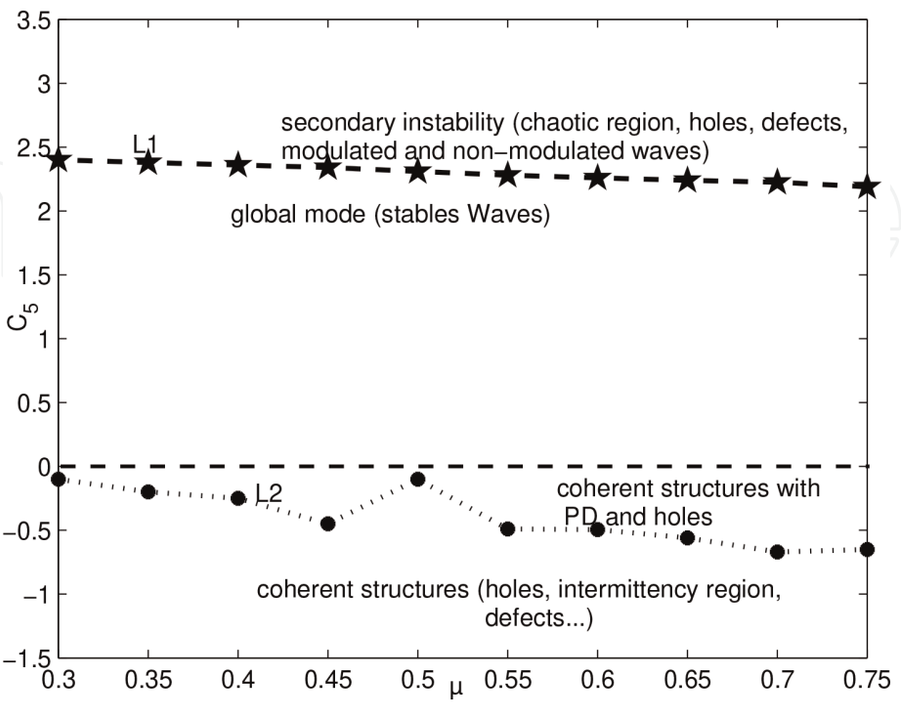


Figure 10.
Phase diagram in (μ,c_5), with $c_1 = 0.45$, $c_3 = 2.0$, $c_5 = 2.0$, $L = 100$, and $v = 1.0$. PD and PH stand for periodic defects and periodic hole regions, respectively.

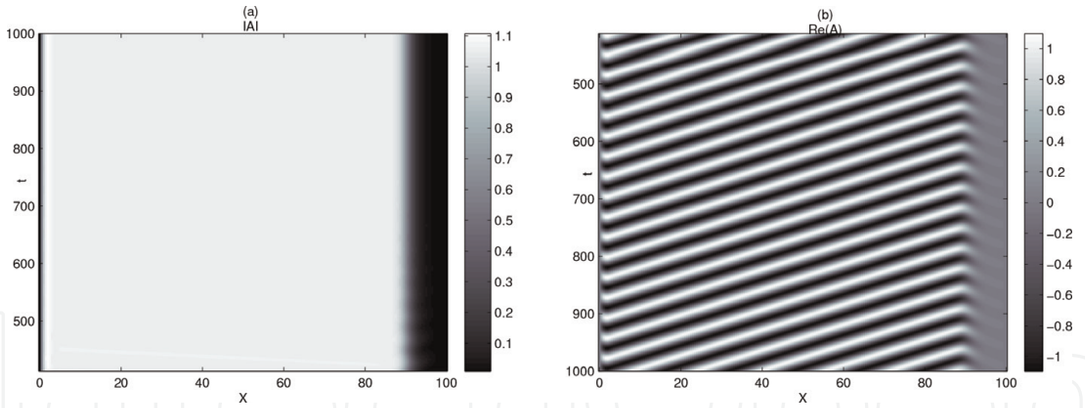


Figure 11.
Space-time variation of the Re(A) for $\mu = 0.3$, $c_1 = 0.450$, $c_3 = 2.0$, $c_5 = 2.0$, $L = 100$ and $\nu = 1$, showing global modes.

downstream boundary. The global mode regime is represented by the phase plots in **Figure 11**. This figure demonstrates the selection of the stable waves in the global mode. It reveals that the wave patterns are decreasing in time and propagate in only one direction toward the left. The variation of the coefficient c_5 leads to bifurcation of the global mode to new states which is observed in **Figure 12**. It reveals that the solution can break up into several disjoint states with different properties separated by more fronts defined by the location of the states. The regular pattern is destabilized and gives rise to spatiotemporal turbulent state near the wall $x = 0$ (space x_1), which is followed by a modulated state in space and time (space x_2), while, near the end $x = L$, the wave pattern remains non-modulated, and the regular wave train is observed (space x_3) [18, 37]. Defect and holes can be detected in the chaotic space. Defects and holes are local structures that play a crucial role in the intermediate regime between laminar states and hard chaos. Defects are points in the space-time diagram where the amplitude of the wave vanishes and the phase is not defined. In two and higher dimensions, such defects can disappear only via collisions with other defects and act as long-living seeds for local structures like spirals [38]. We have noticed that when c_5 further increases, the chaotic region

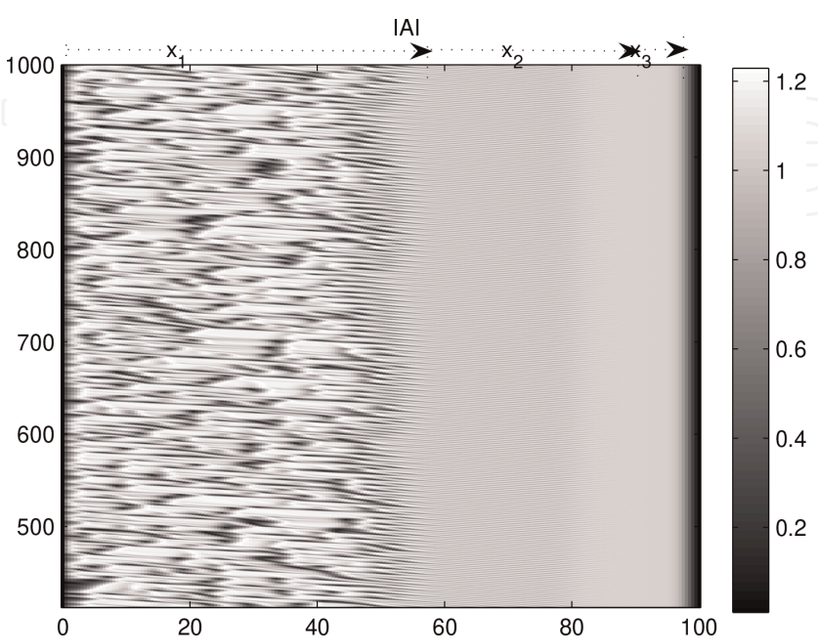


Figure 12.
Space-time variation of the wave pattern amplitude $|A|$, for $\mu = 0.65$, $c_1 = 0.450$, $c_3 = 2.0$, $c_5 = 2.37$, $L = 100$, and $\nu = 1$, indicating the appearance of the secondary structures.

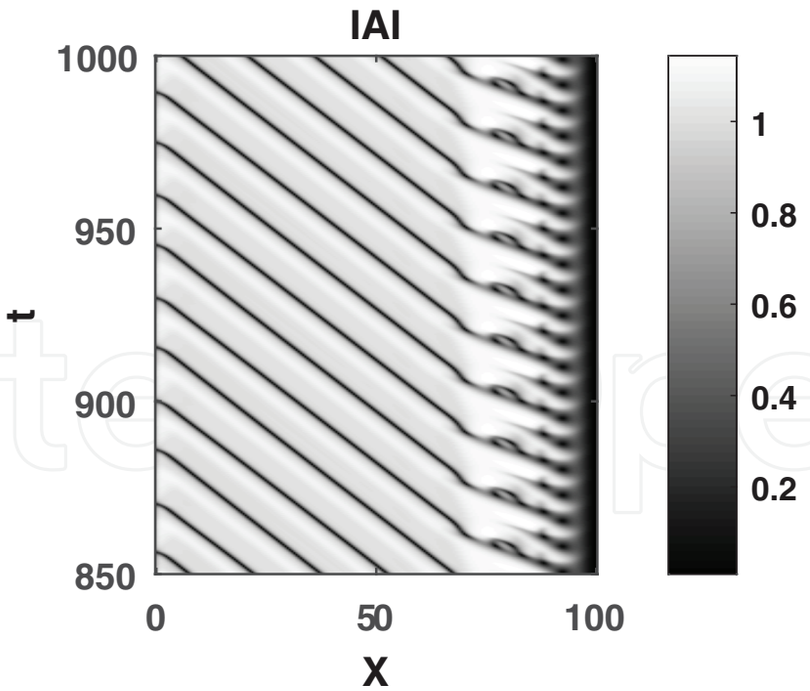


Figure 13.
Space-time variation of the wave amplitude |A|, for $\mu = 0.35$, $c_1 = 0.450$, $c_3 = 2.0$, $c_5 = ?0.2$, $L = 100$, and $\nu = 1$, denoting coherence structure with PD and PH.

propagates into the domain toward the upstream boundary and the system becomes more and more chaotic. For negative values of c_5, the regimes observed are different. The domain exhibits global modes, amplitude defects, holes, and spatiotemporal intermittency. **Figure 13** reveals that the wave patterns are stable at the first part of the domain until the three quarter of the domain. Near the upstream boundary, the news structures are revealed (hole, defects, etc.). The defects appear at regular time intervals around x = 80, and for this reason we call them time-periodic defects (PD). The periodic topological defects have been observed, for example, in many experiences like the miscible fluid convection [39] and the system of Taylor-Dean [40]. Near the right boundary, holes are observed and also before the PD, around

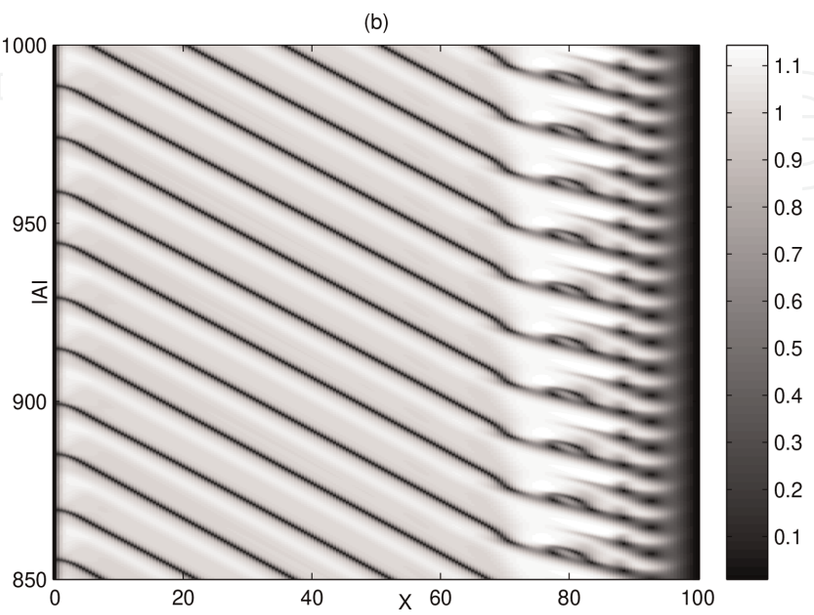


Figure 14.
Space-time variation of the wave pattern amplitude |A| showing also coherence structures with PD and PH, for $\mu = 0.3$, $c_1 = 0.450$, $c_3 = 2.0$, $c_5 = ?\ 0.25$, $L = 100$, and $\nu = 1$.

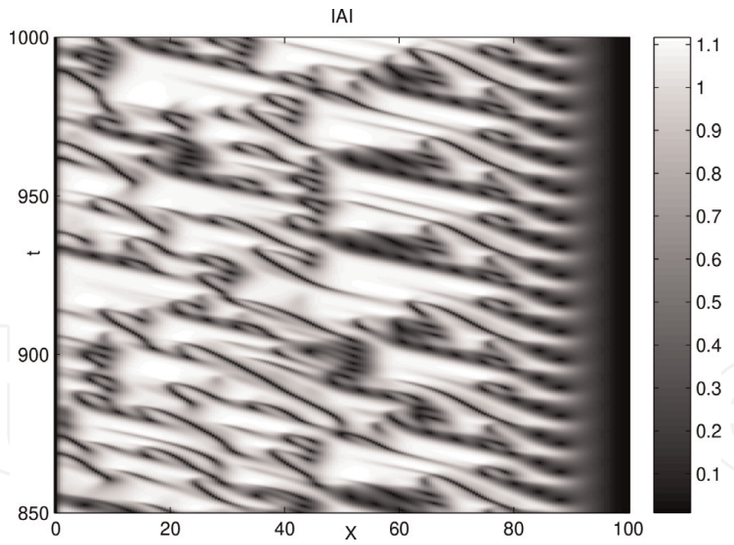


Figure 15.
Space-time variation of the wave pattern amplitude |A|, for $\mu = 0.3$, $c_1 = 0.450$, $c_3 = 2.0$, $c_5 = ?0.6$, $L = 100$, and $\nu = 1$, displaying spatiotemporal intermittency, defects, and holes.

x = 70. Holes which appear near the upstream boundary are regular in time interval, and we call them periodic holes (PH). **Figure 14** is obtained for another value of c_5. It shows a periodic sequence of phase jumps propagating in the advection direction, i.e., to the left; the wave pattern amplitude is modulated in this region. We notice that periodic defects and periodic holes are advected toward the upstream boundary. For the increasing values of c_5, the space-time of **Figure 15** reveals that the system becomes a more disordered regime and more complex. This space-time reveals the disordered regimes in the domain and the behavior of the patterns become more complex. The figure reveals the presence of the core of defects around x = 85 which are periodic. Before the periodic defects, a disordered regime is observed. This disordered regime is a spatiotemporal intermittency regime.

4. Controlling spatiotemporal chaos in one-dimensional systems near subcritical bifurcation

4.1 The dynamical model

The modified cubic-quintic CGLE is given by [20]:

$$\frac{\partial A}{\partial t} = \left(1 + ic_1 + \lambda\left(\frac{|A|^2}{|A_0|^2} - 1\right)\right)\frac{\partial^2 A}{\partial x^2} + \mu A + (1 - ic_3)|A|^2 A - (1 - ic_5)|A|^4 A, \tag{7}$$

where $\lambda = \lambda_r + i\lambda_i$ is a complex constant. Notice that the term $\lambda\left(\frac{|A|^2}{|A_0|^2} - 1\right)$ vanishes identically for $A = A_0$. The added term also preserves the phase invariance of the solution of the original cubic-quintic CGLE, $A \rightarrow Ae^{i\phi}$, with ϕ being an arbitrary phase.

4.2 Numerical simulation

We start by assuming that the system is in a deeply chaotic region, i.e., parameters are chosen from defect turbulence area in order to verify the results obtained from the linear stability analysis. **Figure 16** plots the trajectory in phase space, in

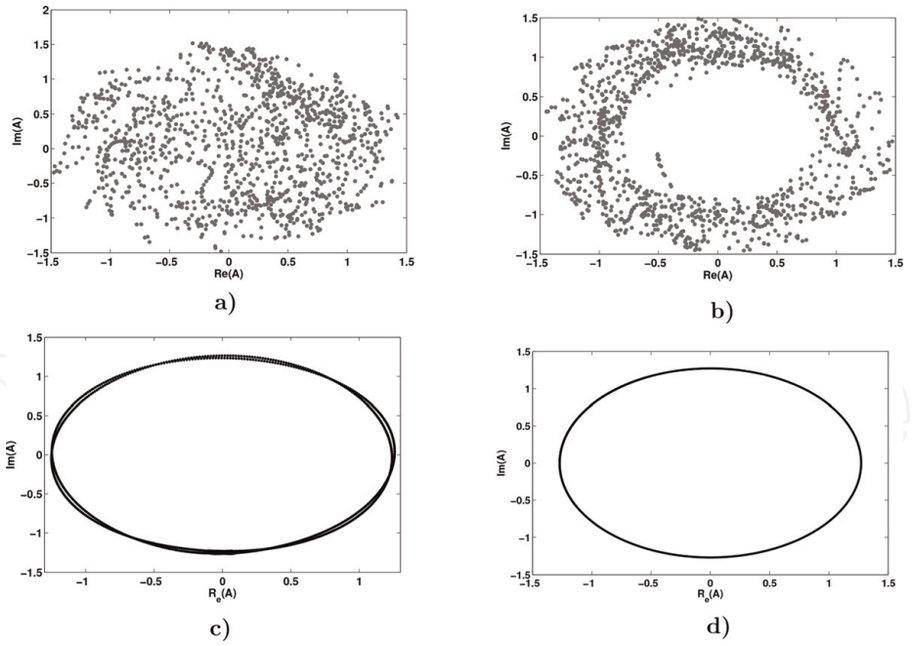


Figure 16.
Plot of (k, c_1) for $c_3 = 0.5$, $c_5 = 1.1$ with (a) $\lambda_r = 0.0$, et $\lambda_i = 0.0$, (b) $\lambda_r = 1.0$, et $\lambda_i = 0.0$, (c) $\lambda_r = 2.5$, et $\lambda_i = 1.1$, (d) $\lambda_r = 3.0$, et $\lambda_i = 1.5$, with $\sigma = 0.008$, $k = 0.85$, the dashed lines correspond to the BFN line of the original cubic-quintic CGLE, the solid lines correspond to the BFN line of the modified cubic-quintic CGLE. The shadowed region corresponds to the stability region.

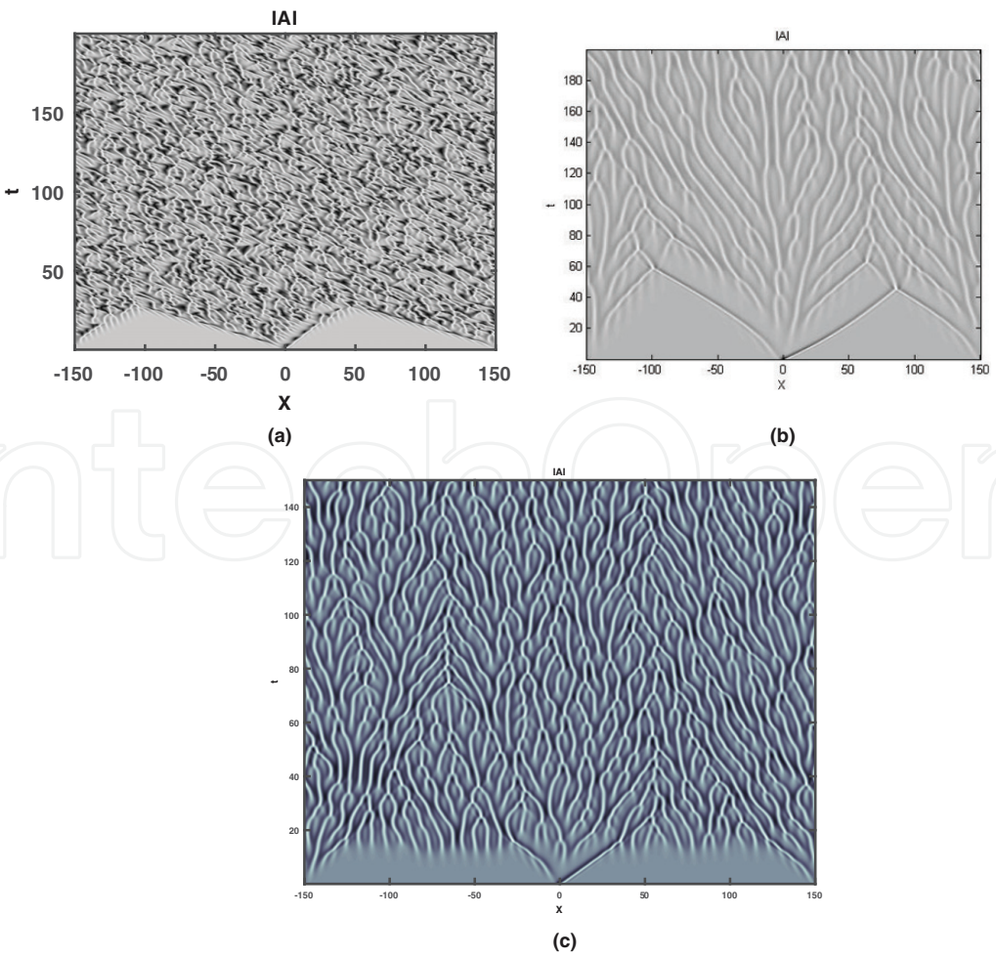


Figure 17.
Transition from chaotic behavior to quasi-periodic state for $c_1 = 2.5$, $c_3 = 0.5$, $c_5 = 1.1$: When (a) $\lambda_r = 0$ and $\lambda_i = 0$ (chaos with defects); (b) $\lambda_r = 2.0$ and $\lambda_i = 0.5$ (phase turbulence); (c) (plane wave) $\lambda_r = 3.2$ and $\lambda_i = 1.8$, with $\sigma = 0.008$, $k = 0.85$, and $N = 1200$ grid points, leading to the plane wave regime.

which the system parameters are exemplified as $c_1 = 2.5$, $c_3 = 0.5$, and $c_5 = 1.1$ [15]. The chaotic motion is obvious: the amplitude of variable incidentally drops to zero to produce defects (see **Figure 16a**). Now we control spatiotemporal chaos by performing nonlinear diffusion parameters. As an example, we let $\lambda_r = 2.0$ and $\lambda_r = 0.5$; the trajectory of system is illustrated in **Figure 16b**. The real part of system variable is confined into a finite range, and defect turbulence is no longer being observed, whereas the chaotic motion is not eliminated completely. For other values of the diffusion parameter as $\lambda_r = 3.0$ and $\lambda_r = 1.5$, for example, the chaotic motion is suppressed, and period-doubled states are observed as is illustrated in **Figure 16c**. The solution has double periodicity since double loop is observed. For the value of λ being more larger, the chaotic motion is still suppressed, but the periodic states are observed. The system is more stable. The double loop is merged into a single loop, as is shown in **Figure 16d**. To get also an idea of how the spatiotemporal dynamics of the system changes in the parameter range of $|\lambda|$ between turbulence and uniform oscillations, we show in **Figure 17a** a series of space-time plots of asymptotic dynamical states reached for different values of $|\lambda|$. For the increasing values of $|\lambda|$, the transition from defect turbulence to plane wave regime is observed (**Figure 17a–c**).

5. Time-delay auto-synchronization control of defect turbulence in cubic-quintic complex Ginzburg-Landau equation

5.1 Model equation

To control the different turbulence regimes observed in the domain, a global feedback term can be introduced. The modified cubic-quintic CGL eqiuation is given by [27, 41, 42].

$$\frac{\partial A}{\partial t} = (1 + ic_1)\frac{\partial^2 A}{\partial x^2} + \mu A + (1 - ic_3)|A|^2 A - (1 - ic_5)|A|^4 A + F, \tag{8}$$

$$F(t) = \alpha e^{i(\chi_0 + \omega\tau)}\overline{A}(t - \tau), \tag{9}$$

where

$$\overline{A}(t) = \frac{1}{L}\int_0^L A(x,t)dx \tag{10}$$

denotes the spatial average of A over a one-dimensional medium of length L. The parameter α describes the feedback strength, and χ_0 characterizes a phase shift between the feedback and the dynamics. ω denotes the frequency of the oscillation and τ is the delay time. When delay time is short $(\tau << 1)$, the slowly varying average amplitude $\overline{A}(t)$ does not significantly change within the delay time, and the delays in this term could be neglected. We obtain then the following equation:

$$\frac{\partial A}{\partial t} = (1 + ic_1)\frac{\partial^2 A}{\partial x^2} + \mu A + (1 - ic_3)|A|^2 A - (1 - ic_5)|A|^4 A + \alpha e^{i\chi}\overline{A}(t), \tag{11}$$

where $\chi = \chi_0 + \omega\tau$. Eq. (11) does not include any delay. Nonetheless, the delay time τ plays an important role here, because it determines the effective phase shift χ in the equation. The variation of τ provides a simple way for changing the phase shift of the global feedback and thus the feedback effects.

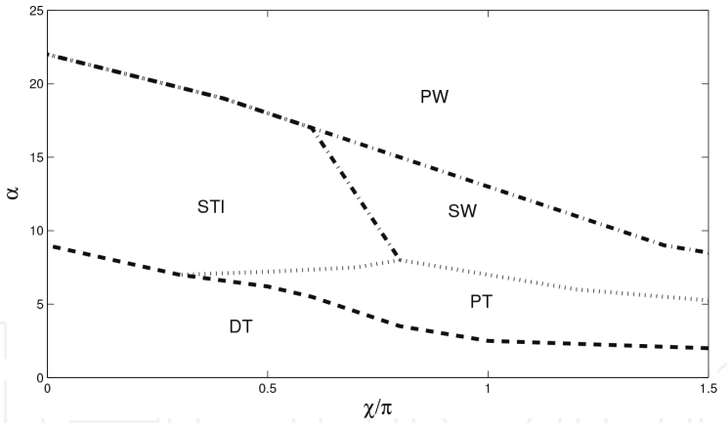


Figure 18.
Phase diagram of (χ, α) showing different types of dynamical regimes: Defect turbulence (DT), spatiotemporal intermittency (STI), phase turbulence (PT), standing wave (SW), and plane wave (PW) for $c_1 = 2.5$, $c_3 = 0.5$, $c_5 = 1.1$. Phase diagram of (χ, α) showing different types of dynamical regimes: Defect turbulence (DT), spatiotemporal intermittency (STI), phase turbulence (PT), standing wave (SW), and plane wave (PW) for $c_1 = 2.5$, $c_3 = 0.5$, $c_5 = 1.1$, $\mu = 1.0$, $\mu = 1.0$.

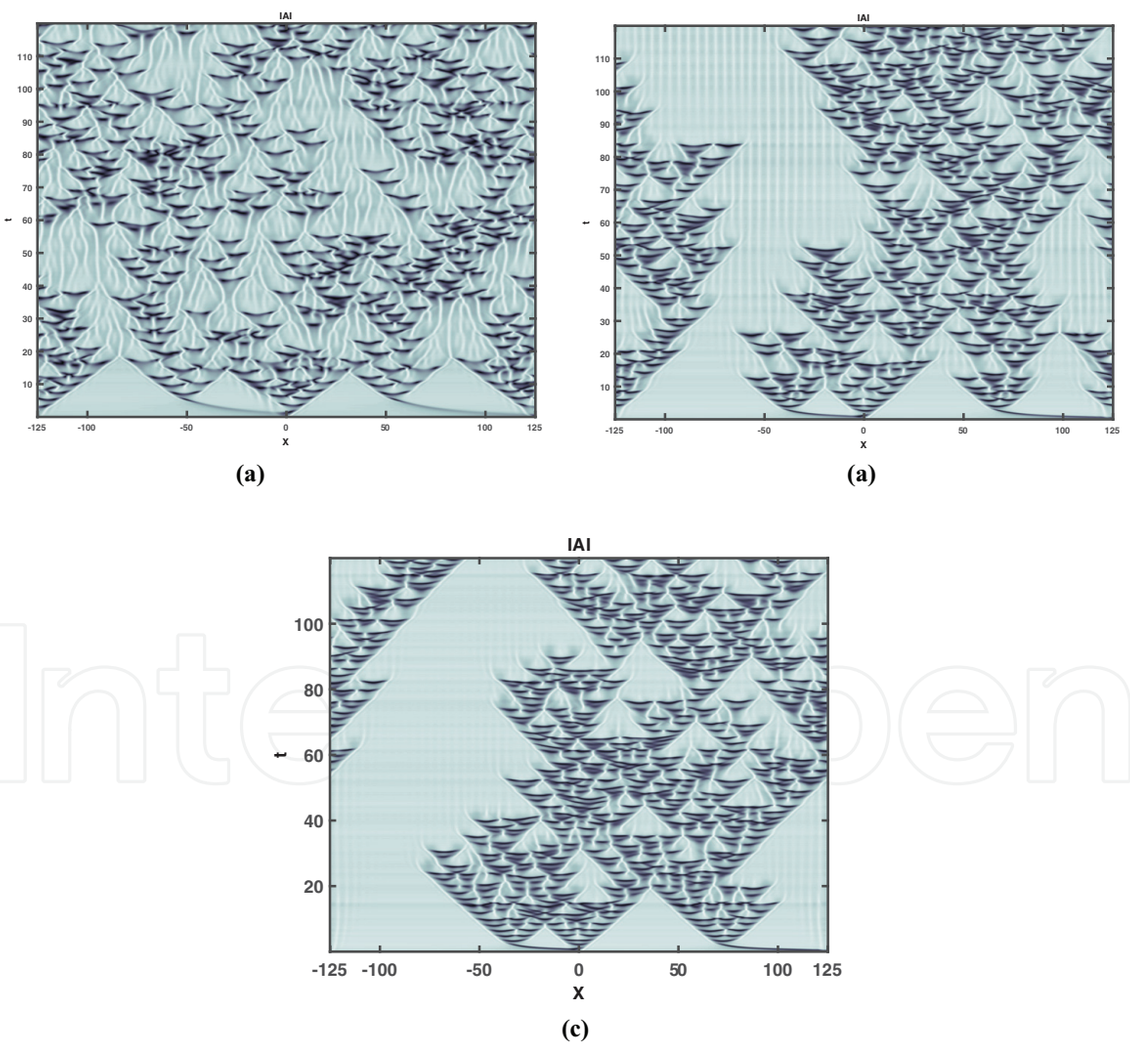


Figure 19.
Transition from defect turbulence to spatiotemporal intermittency regime for $c_1 = 2.5$, $c_3 = 0.5$, $c_5 = 1.1$, $\chi = \pi/6$, and $\mu = 1.0$, when (a) $\alpha = 8.0$, (b) $\alpha = 12.0$, (c) $\alpha = 15$.

5.2 Numerical simulation

In this section, we present the results of a numerical study of Eq. (11). We analyze the stability of the unstable wave patterns observed inside a defect

turbulence regime by using global feedback term [27]. We study the effects of the feedback term on the system. A sufficient strong feedback can suppress spatiotemporal chaos and establishes uniform oscillations. We show that for certain values of the global feedback term and the delay time, the system which initially was chaotic becomes completely stable. The dynamic regimes observed during the numerical study are summarized in the state diagram of **Figure 18**. The five regimes observed are defect turbulence, spatiotemporal intermittency, phase turbulence, standing waves, and plane waves. We remark that as the feedback intensity is increased starting from zero, global oscillations set in, and defect turbulent regimes are replaced by other interesting regimes until the appearance of the laminar state.

For certain values of α, amplitude defects disappear from some parts of the system, and thus, an intermittent state is developed. **Figure 19** illustrates three examples of intermittent regimes depending on the values of α and χ in a 1D system [27, 42]. **Figure 19a** shows that turbulent bursts which occupy most of the system and laminar areas are relatively rare, while **Figure 19b** and **c** shows the coexistence between turbulence and laminar state filled with standing wave (see **Figure 19b**) or plane waves (see **Figure 19c**). By further increasing the feedback intensity from the states of intermittent turbulence, uniform oscillations are observed for the phase shift in the interval $0 < \chi < 3\pi/4$. For appropriate values of α and χ, the domain is still always turbulent, but the defects disappeared completely. The wave pattern is

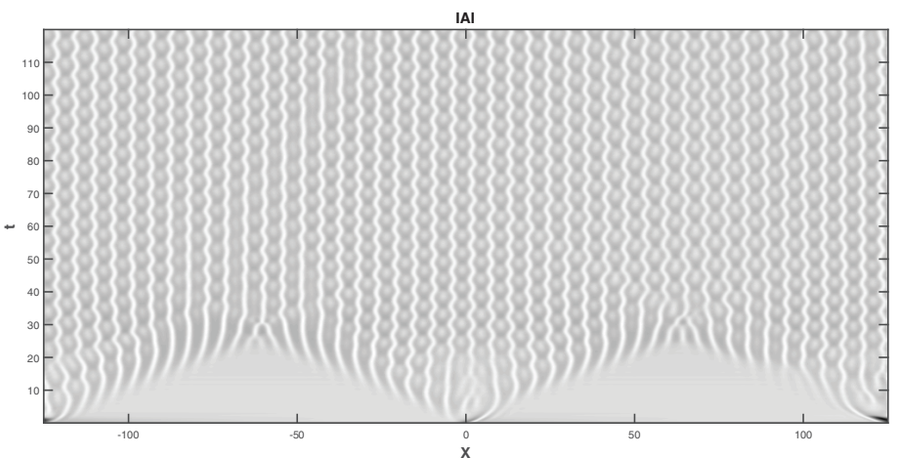


Figure 20.
Phase turbulence regime of wave pattern amplitude $|A|$ obtained for $\alpha = 6.0$, $c_1 = 2.5$, $c_3 = 0.5$, $c_5 = 1.1$, $\chi = 7\pi/4$, $\mu = 1.0$.

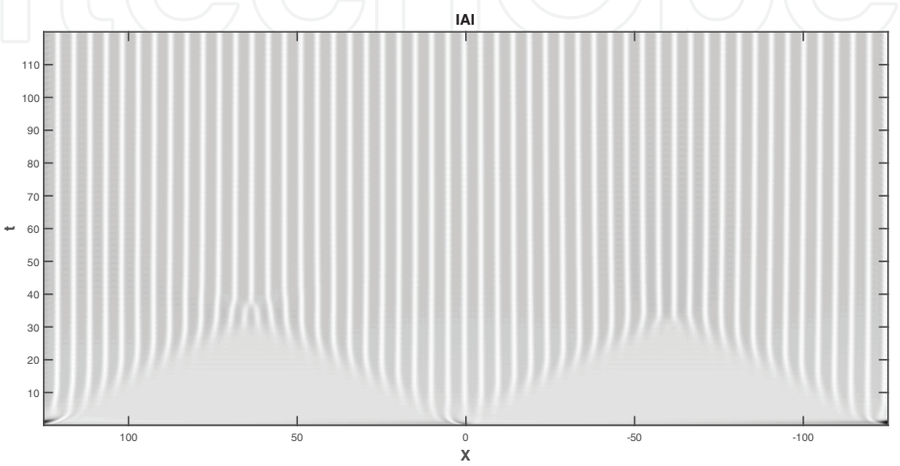


Figure 21.
Space-time variation of the wave pattern amplitude $|A|$ obtained for $\alpha = 9.0$, $c_1 = 2.5$, $c_3 = 0.5$, $c_5 = 1.1$, $\chi = 7\pi/4$, $\mu = 1.0$.

in the phase turbulence regime. It is illustrated in **Figure 20**. In this regime, the amplitude is always bounded away from zero. The amplitude A never reaches zero and remains saturated. We notice that for certain values of α and χ, standing waves, also called stationary wave, are observed (see **Figure 21**). Standing waves have been observed in the model of CO oxidation under intrinsic gas phase coupling [43, 44].

6. Discussion

Let us now introduce to the CGL equation the global time-delay feedback and study its effects on the system. The new CGL equation with time-delay auto-synchronization is given by:

$$\frac{\partial A}{\partial t} = (1 + ic_1)\frac{\partial^2 A}{\partial x^2} + (\mu - i\omega)A + (1 - ic_3)|A|^2 A - (1 - ic_5)|A|^4 A + F, \qquad (12)$$

where F is a feedback term given by

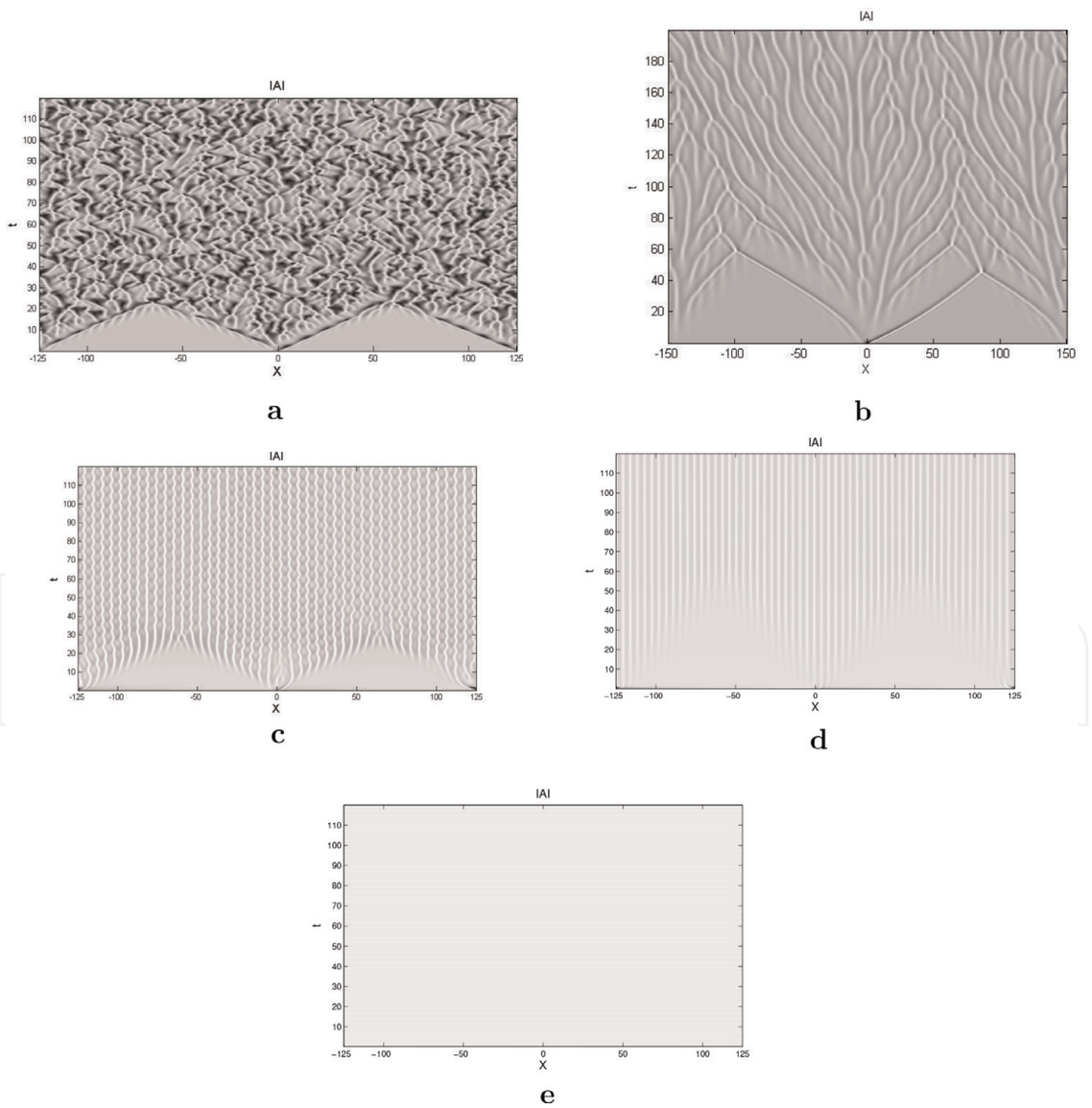


Figure 22.
Space-time variation of the wave pattern amplitude $|A|$, $\chi = \pi/2$, $c_1 = 2.5$, $c_3 = 0.5$, $c_5 = 1.1$, $\mu = 1.0$, and $\tau = 1.2$ for (a) $\alpha = 0.0$ showing DT, (b) $\alpha = 12.0$ showing WT, (c) $\alpha = 15$ showing PT, and $\alpha = 15$ showing PW.

$$F(t) = \alpha e^{i\chi}\left(\overline{A}(t-\tau) - \overline{A}(t)\right), \tag{13}$$

and

$$\overline{A}(t) = \frac{1}{L}\int_0^L A(x,t)dx, \tag{14}$$

with the amplitude and frequency given by

$$|A_1|^2 = \frac{1}{2}\left(1 \pm \sqrt{1 + 4(\mu + \alpha[\cos(\chi - \Omega\tau) - \cos(\chi)])}\right), \tag{15}$$

and

$$\Omega = -\omega - |A_1|^2\left(c_3 - c_5|A_1|^2\right) + \alpha[\sin(\chi - \Omega\tau) - \sin(\chi)]. \tag{16}$$

A cubic CGL equation with a similar feedback scheme has been investigated in Refs. [13, 35]. In their work, they have shown how the strongly disordered state can be stabilized in the system. The initially unstable system undergoes several transformations successively and become stable; we have in order defect turbulence, phase turbulence, standing wave state, and uniform oscillations. The results of our numerical study of Eq. (12) are given in **Figure 22**. This figure shows the progressive transition from defect turbulence to plane wave state. In the absence of feedback (see **Figure 22a**, with α = 0), defect turbulence is observed. For small α, weak turbulence is observed (see **Figure 22b**). When the feedback term grows, the system displays a disordered state of phase turbulence (see **Figure 22c**), stationary standing wave patterns (see **Figure 22d**), and uniform oscillations (see **Figure 22e**), respectively.

7. Effects of nonlinear gradient terms on the defect turbulence regime in weakly dissipative systems

The LOCGL equation which describes a system exhibiting a subcritical bifurcation to traveling waves must contain a quintic nonlinearity; at this order, it is necessary to include the lower-order nonlinear gradient terms:

$$\begin{aligned} A_t + VA_x = (\chi_r + i\chi_i)A + (1 + ic_1)A_{xx} + (1 - ic_3)|A|^2A - \\ (1 - ic_5)|A|^4A - q_1|A|^2A_x - q_2|A|_x^2A - q_3A^2A_x^*, \end{aligned} \tag{17}$$

with $q_1 = q_{1r} + iq_{1i}$, $q_2 = q_{2r} + iq_{2i}$, and $q_3 = q_{3r} + iq_{3i}$. Here, $A(x,t)$ describes the amplitude of extended spatial patterns. The values q_1, q_2, and q_3 represent coefficients of nonlinear gradient terms. Two of these nonlinear gradient terms, i.e., $|A|^2A_x$ and $A^2A_x^*$, appear naturally in the asymptotic derivation [30, 31, 45–47]. Since we take the periodic boundary conditions, the convective term VA_x may be transformed away by going into a moving frame of reference. Also, the parameter $\chi = \chi_r + i\chi_i$, which is proportional to the distance from criticality, can be taken as real, since the imaginary part can be transformed away by a simple transformation.

The aim is to see the impact of these nonlinear gradient terms on a defect turbulence regime. We use the indicators such as the Lyapunov exponent and the energy bifurcation diagram to confirm the nature of the regime.

7.1 Numerical simulations

7.1.1 Dynamical indicators

We will essentially characterize the different types of dynamical behavior of the system by the energy function Q and the largest Lyapunov exponent λ_{max}. The first one is defined by

$$Q(t) = \frac{1}{2L}\int_{-L}^{L} |A(x,t)|^2 dx, \tag{18}$$

which is frequently used to characterize non-regular dynamics in optics [48], localized patterns in fluids, and other physical systems, respectively [49]. The one-dimensional system is assumed to be of length $2L$. In order to check more dynamical behaviors of the system and provide a more quantitative aspect of the dynamics, we calculate the largest Lyapunov exponent defined by [50, 51].

$$\lambda_{max} = \lim_{t\to\infty}\left[\frac{1}{t}\ln\left(\frac{|||\delta A(x,t)|||}{|||\delta A(x,0)|||}\right)\right], \quad with \quad \|\delta A(x,t)\| = \left\{\int_{x=-L}^{x=L} |\delta A(x,t)|^2 dx\right\}^{1/2}, \tag{19}$$

where δA is a small perturbation such as $A = A_0 + \delta A$ and A_0 is the initial value of the amplitude wave. Here, $\delta A(x,0) = 10^{-4}A_0$, and δA satisfies the linearized evolution equation

$$\frac{\partial \delta A}{\partial t} = \bar{\mathbf{J}} \cdot \delta A, \tag{20}$$

where $\bar{\mathbf{J}}$ is the Jacobian matrix. The largest Lyapunov exponent is the dynamical invariant most easily and accurately estimated from experimental time series. This method has been extensively used for many different dynamical systems to quantify chaos [30]. The value λ_{max} can be positive or negative. Complex behaviors such as chaos and spatiotemporal chaos are confirmed by positive λ_{max}. On the other hand, periodic or quasi-periodic solutions and non-chaotic attractors are characterized by negative λ_{max}.

7.1.2 Numerical results

We will present here some of data obtained for systems with the presence of the nonlinear gradient terms. The results are summarized in **Figures 23–28**. In particular, we study the influence of the nonlinear gradient terms in the defect turbulence regime. **Figure 23** shows the wave patterns and the energy as a function of time corresponding to the laminar regime. We notice that the system that was initially chaotic becomes completely stable by the presence of the nonlinear gradient terms. The chaos has been eliminated. By changing the values of nonlinear gradient terms, the dynamics of the system also change; it is confirmed by **Figures 24** and **25** which represent the oscillating patterns. The corresponding largest Lyapunov exponent is zero.

The plot observed in **Figure 24** is the running waves. They are quasi-periodic states; they move in one direction with constant speed, according to its initial condition; and this is the so-called oriental symmetry breaking. A double periodicity in time and in space is observed. In **Figure 25**, we have another type of the

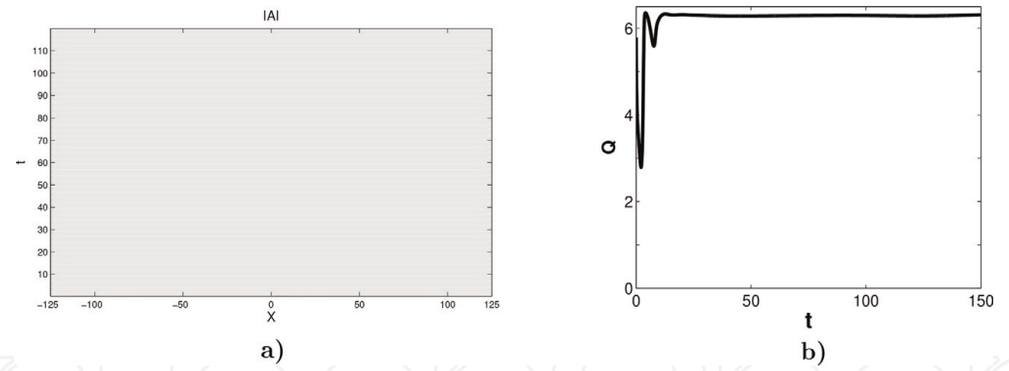


Figure 23.
(a) Laminar regime and (b) pattern energy Q, as function of time for $q_1 = 1.5 + 0.5i$, $q_2 = q_3 = 1.5 + 1.5i$.

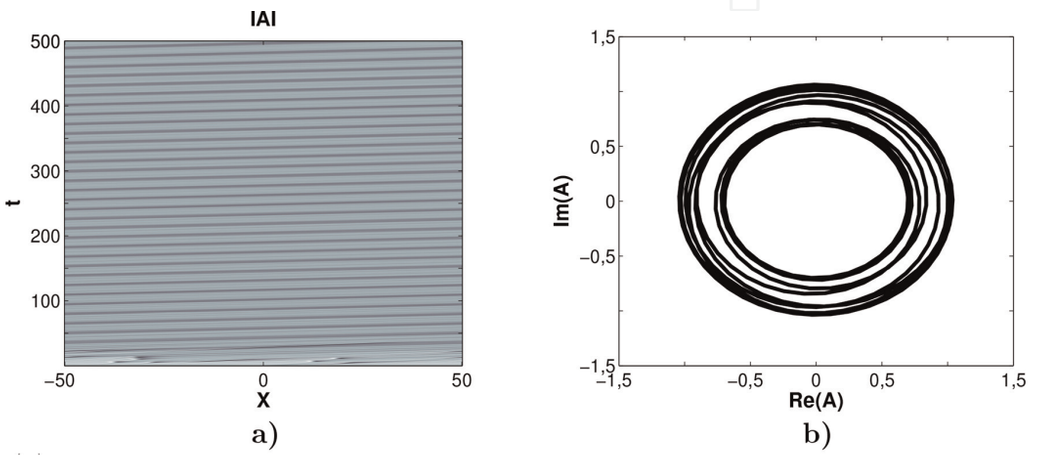


Figure 24.
(a) Running wave regime, for $\chi = 0.6$ $q_1 = 0.5 + 0.9i$, $q_2 = 0.6 + 0.6i$, $q_3 = 0.9 + 0.9i$, and (b) phase portrait of running waves.

oscillating patterns in a color-coded space-time plot (see **Figure 25a**). After a transient time, the waves propagate uniformly, with a well-defined wave number and constant amplitude. We note also the presence of an attractor into the system which annihilate the wave patterns (see **Figure 25b**). The drop observed near $x = 0$ expresses the fact that the initial condition is a hole. **Figures 26–28** show the largest Lyapunov exponent λ_{max} and the bifurcation diagram of the pattern state as a function of the control parameter χ_r for Eq. (17). They allow us to see clearly how the

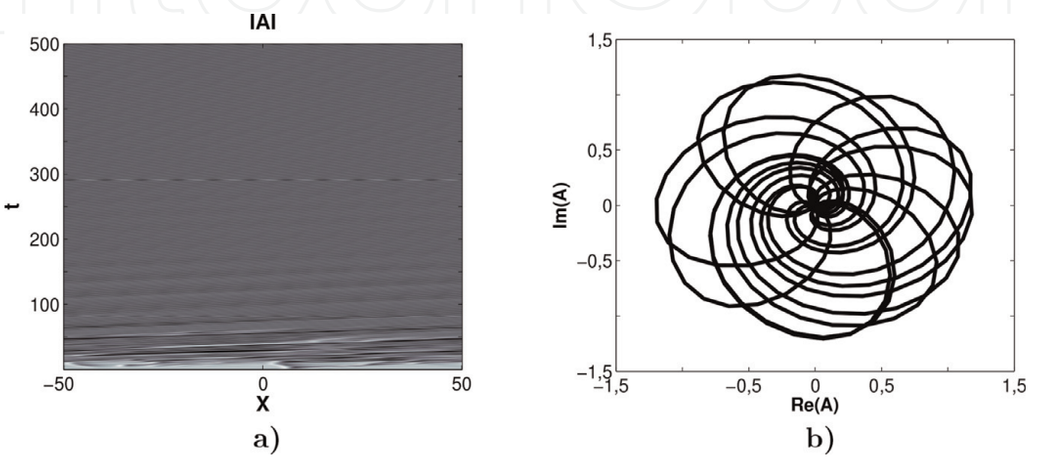


Figure 25.
Oscillating regime in system, for $\chi = 0.6$ $q_1 = 1.5 + 0.5i$, $q_2 = 0.6 + 0.6i$, $q_3 = 1.5 + 0.9i$: (a) space-time plot of $|A|$ propagating in one dimension and (b) phase portrait of wave patterns.

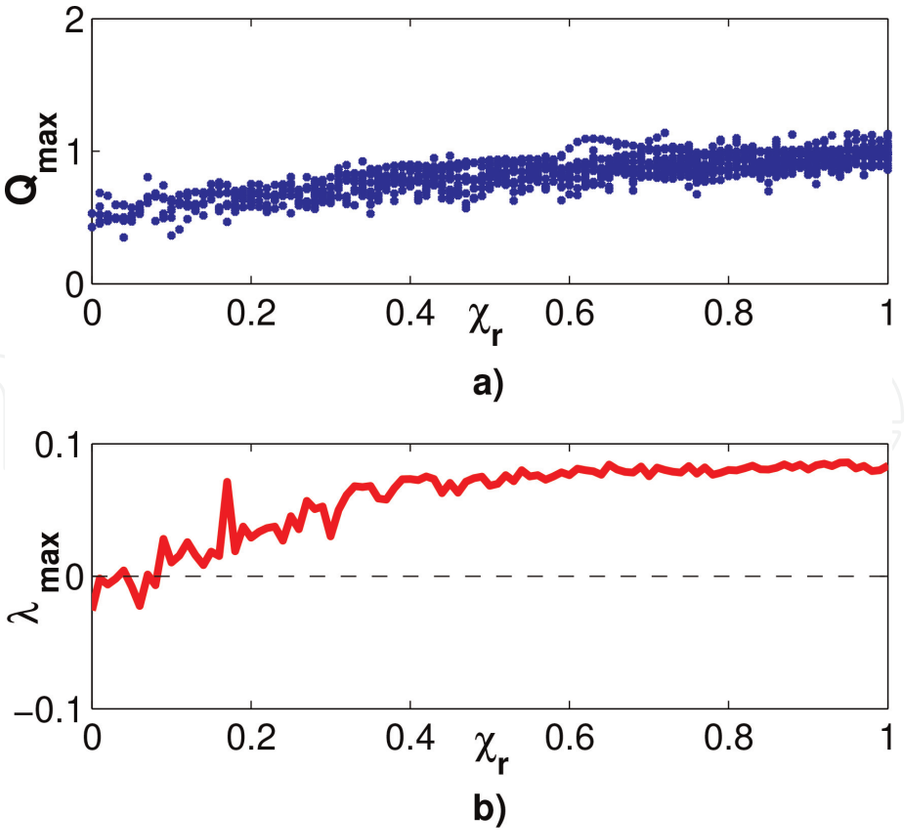


Figure 26.
(a) Bifurcation diagram of Q_{max} and (b) largest Lyapunov exponent λ_{max} as function of χ_r, without nonlinear gradient terms.

system changes its dynamical behavior with the presence of the nonlinear gradient terms. **Figure 26a**, which express the case without the nonlinear gradient terms, is obtained by taking repeatedly the maximum value of the energy function Q_{max} in a

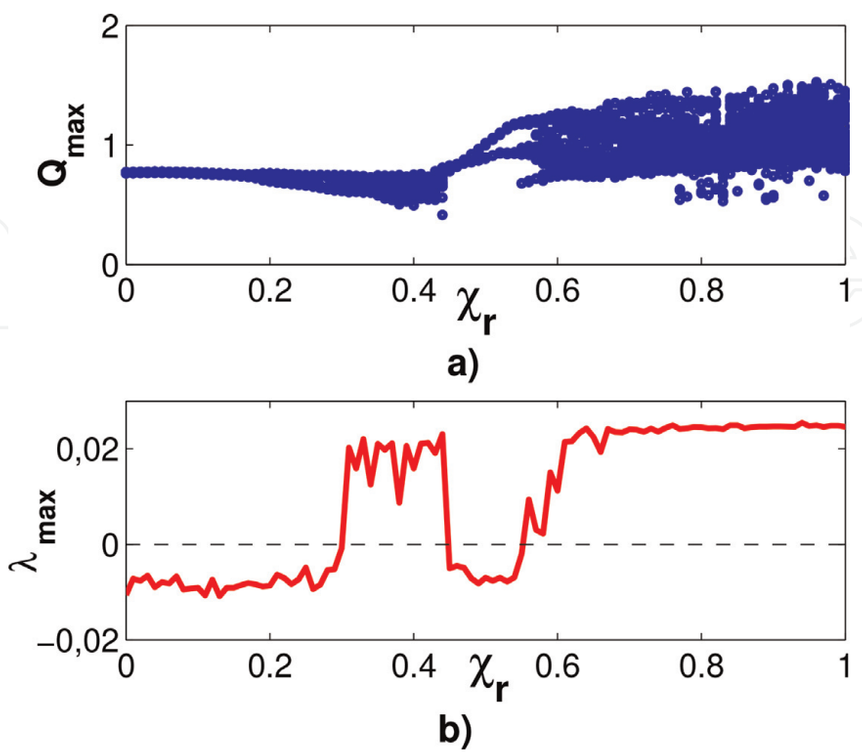


Figure 27.
(a) Bifurcation diagram of Q_{max} and (b) largest Lyapunov exponent λ_{max} as function of χ_r, with $q_1 = 0.1 + 0.1i$, $q_2 = 0.2 + 0.2i$, and $q_3 = 0.3 + 0.3i$.

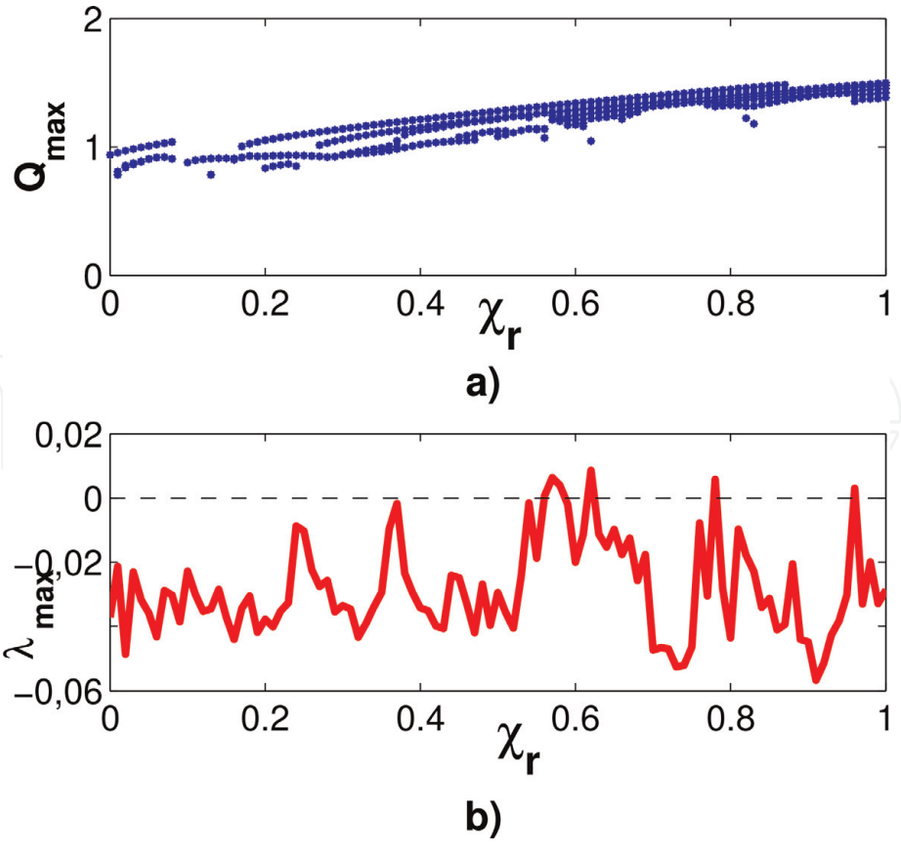


Figure 28.
(a) Bifurcation diagram of Q_{max} and (b) largest Lyapunov exponent λ_{max} as function of χ_r, with $q_1 = 0.7 + 0.7i$.

given time interval at different times (well after the transient is dead); this is done for very many different values of the control parameter χ_r. As can be seen, the system is briefly stable, and then, the instability is present in the whole system. In fact, if there is a unique Q_{max}, then the system is stationary or periodic, while for finite continuous distribution of Q_{max} values, the behavior is either quasi-periodic or chaotic.

The Lyapunov exponent shown in **Figure 26b** indicates the dynamical behavior of the system and confirms the results. **Figure 27** is obtained for increasing values of the nonlinear gradient terms. We observe several transitions between regular and chaotic states. In particular, there is a small stability part of the system in the range $\chi_r \in (0.0, 0.3)$. Beyond the point $\chi_r = 0.44$, the system becomes stable again until the value $\chi_r = 0.55$, with another bifurcation point at $\chi_r = 0.6$. On the other hand, the transition from regular to chaotic wave patterns is flat. In the plot of the Lyapunov exponent (see **Figure 27b**), the chaotic motions identified are validated by the positive values of λ_{max}, while the stable region corresponds to the negative values of λ_{max}. For the large value of the nonlinear gradient terms, the system becomes more and more stable as is seen in **Figure 28**.

8. Conclusion

The numerical investigation of the 1D quintic CGL equation in such systems represents a big topic in the understanding of many physical systems with pattern formation. Concerning the extended system, we have summarized in a phase diagram all the regimes that have been observed. On the phase diagram, we have the BFN line that divides the regions in two regions: the stable zone which contains laminar state and spatiotemporal intermittency regime and the unstable zone with

chaotic regimes as phase turbulence, weak turbulence, and defect turbulence [49]. For the case of finite system, we have described from the 1D cubic-quintic CGL equation the effects of the boundaries on the waves traveling in a preferred direction. We have used the homogeneous boundary conditions, and the waves were nonlinear dissipative waves. We have studied the nature of convective or absolute instabilities of wave patterns. In our simulations, we have found new states that were similar from those obtained in the cubic CGL equation with homogeneous boundary conditions or with the Neumann boundary conditions. The presence of the quintic term has a large influence in the wave pattern. All the dynamic regimes observed have been summarized in a state diagram. The regimes as the global mode regime, turbulence regime observed in the secondary structures, and spatiotemporal intermittency regimes have been detected, but their shape and behavior are different depending on the sign of c_5. Such defects, holes, and spatiotemporal intermittency regime have been observed in the spiral wave pattern in the counterrotating Couette-Taylor system, in the Taylor-Dean system, and in Rayleigh-Bénard convection. These results were different from those that used periodic boundary conditions. The numerical investigation of the 1D cubic-quintic CGL equation with homogeneous boundary conditions for different values of the control parameters represents a big topic in the understanding of many physical systems with pattern formation. One of the great challenges is to control these instabilities. We have used three types of control. Many significant technological applications, such as mixing, optical fiber manufacture, and chemical reaction could crucially benefit from the control of instabilities leading to complex spatiotemporal dynamics. Firstly, we have proposed a method based on a nonlinear diffusion parameter control which lies to the modified cubic-quintic CGL equation in the extended system. In the first time, we have briefly presented the model equation of cubic-quintic CGL equation and summarized the dynamic regimes observed in the phase diagram of BFN. This method is based on the modification of the nonlinear coefficient term with the preservation of the intrinsic phase invariance of the original equation. By using hole solutions as initial conditions, we have simulated the modified cubic-quintic CGL equation. Then, spatiotemporal chaos regimes obtained with the original cubic-quintic CGL equation have been stabilized by using a nonlinear diffusion term. The results show that, the defect turbulence regime which is initially observed, become progressively stable by modifying the values of the nonlinear diffusion term, i.e., at the end, plane wave regime is observed. Then, by using another type of control called time-delay auto-synchronization, which consists in adding the feedback term to the CGL equation, the results were excellent. We have noticed by this method that one can control or avoid the spatiotemporal chaos observed into the system. The last method control used is the adding of the nonlinear gradient terms to the CGL equation called the lowest-order CGL equation. By considering also the wave patterns in the chaotic regions in particular in a defect turbulence regime, it was shown that the presence of the nonlinear gradient terms changes the dynamical behavior of the system; the chaos can disappear progressively in the domain. The fact that the nonlinear gradient terms can stabilize the system leads us to conclude that they can be considered as the stabilizing terms.

Acknowledgements

The work by CBT is supported by the Botswana International University of Science and Technology under the grant **DVC/RDI/2/1/16I (25)**. CBT thanks the Kavli Institute for Theoretical Physics (KITP), University of California Santa Barbara (USA), for invitation.

IntechOpen

Author details

Joël Bruno Gonpe Tafo[1], Laurent Nana[1], Conrad Bertrand Tabi[2*] and Timoléon Crépin Kofané[3]

1 Laboratoire de Physique Fondamentale, Groupe Phénomènes Non Linéaires et Systèmes Complexes, UFD de Physique Fondamentale et Sciences de l'Ingénieur, Université de Douala, Douala, Cameroun

2 Botswana International University of Science and Technology, Palapye, Botswana

3 Laboratoire de Mécanique, Département de Physique, Faculté des Sciences, Université de Yaoundé I, Yaoundé, Cameroun

*Address all correspondence to: tabic@biust.ac.bw

IntechOpen

© 2020 The Author(s). Licensee IntechOpen. This chapter is distributed under the terms of the Creative Commons Attribution License (http://creativecommons.org/licenses/by/3.0), which permits unrestricted use, distribution, and reproduction in any medium, provided the original work is properly cited. CC BY

References

[1] Cross M, Hohenberg P. Pattern formation outside of equilibrium. Reviews of Modern Physics. 1993;**65**:851

[2] Lega J. Traveling hole solutions of the complex Ginzburg–Landau equation. Physica D: Nonlinear Phenomena. 2001; **152**:269

[3] Coullet P, Gil L, Lega J. Defect-mediated turbulence. Physical Review Letters. 1989;**62**:1619

[4] Nana L, Ezersky AB, Abcha N, Mutabazi I. Dynamics of spatio-temporal defects in the Couette-Taylor flow: Comparison of experimental and theoretical results. Journal of Physics: Conference Series. 2008;**137**:012006

[5] Kodama Y, Hasegawa A. Generation of asymptotically stable optical solitons and suppression of the Gordon–Haus effect. Optics Letters. 1992;**17**:31

[6] Lee KJ, McCormick WD, Ouyang Q, Swinney HL. Experimental observation of self-replicating spots in a reaction-diffusion system. Nature (London). 1994;**369**:215

[7] Bramwell ST, Holdsworth PCW, Pinton JF. Universality of rare fluctuations in turbulence and critical phenomena. Nature (London). 1998; **396**:552

[8] Kuramoto Y. Chemical Oscillations, Waves, and Turbulence. Berlin: Springer; 1984

[9] Kim M, Bertram M, Pollmann M, von Oertzen A, Mikhailov AS, Rotermund HH, et al. Controlling chemical turbulence by global delayed feedback: Pattern formation in catalytic co oxidation on pt(110). Science. 2001; **292**:1357

[10] Sinha S, Pande A, Pandit R. Defibrillation via the elimination of spiral turbulence in a model for ventricular fibrillation. Physical Review Letters. 2001;**86**:3678

[11] Aranson IS, Kramer L. The world of the complex Ginzburg–Landau equation. Reviews of Modern Physics. 2002;**74**:99

[12] Lega J, Fauve S. Traveling hole solutions to the complex Ginzburg–Landau equation asperturbations of nonlinear Schrödinger dark solitons. Physica D: Nonlinear Phenomena. 1997; **102**:234

[13] van Hecke M. Building blocks of spatiotemporal intermittency. Physical Review Letters. 1998;**80**:1896

[14] Descalzi O, Gutiérrez P, Tirapegui E. Localized structures in nonequilibrium systems. International Journal of Modern Physics C. 2005; **16**:1909

[15] Gonpe Tafo JB, Nana L, et L, Kofane TC. Dynamics of a traveling hole in one-dimensional systems near subcritical bifurcation. The European Physical Journal Plus. 2011;**126**:105

[16] Nana L, Ezersky AB, Mutabazi I. Secondary structures in a one-dimensional complex Ginzburg-Landau equation with homogeneous boundary conditions. Proceedings of the Royal Society A. 2009;**465**:2251

[17] Descalzi O, Brand HR. Influence of Dirichlet boundary conditions on dissipative solitons in the cubic-quintic complex Ginzburg-Landau equation. Physical Review E. 2010;**81**:026210

[18] Gonpe Tafo JB, Nana L, Kofane TC. Nonlinear structures of traveling waves in the cubic–quintic complex Ginzburg–Landau equation on a finite domain. Physica Scripta. 2013;**87**:065001

[19] Schuster H. Handbook of chaos control: Foundations and applications. 1st ed. Weinheim: Wiley-VCH; 1999

[20] Gonpe JB, Nana L, Kofane TC. Nonlinear diffusion control of defect turbulence in cubic-quintic complex Ginzburg-Landau equation. The European Physical Journal Plus. 2012; **127**:75

[21] Roy R, Murphy T, Maier T, Gills Z, Hunt E. Dynamical control of a chaotic laser: Experimental stabilization of a globally coupled system. Physical Review Letters. 1992;**68**:1259

[22] Hunt E. Stabilizing high-period orbits in a chaotic system: The diode resonator. Physical Review Letters. 1991;**67**:1953

[23] Ditto W, Rauseo S, Spano M. Experimental control of chaos. Physical Review Letters. 1990;**65**:3211

[24] Ott E, Grebogi C, Yorke JA. Controlling chaos. Physical Review Letters. 1990;**64**:1196

[25] Pyragas K. Continuous control of chaos by self-controlling feedback. Physics Letters A. 1992;**170**:421

[26] Pyragas K, Tamaševičius A. Experimental control of chaos by delayed self-controlling feedback. Physics Letters A. 1993;**180**:99

[27] Gonpe Tafo JB, Nana L, Kofane TC. Time-delay autosynchronization control of defect turbulence in the cubic-quintic complex Ginzburg-Landau equation. Physical Review E. 2013;**88**:032911

[28] Deissler RJ, Brand HR. The effect of nonlinear gradient terms on breathing localized solutions in the complex Ginzburg-Landau equation. Physical Review Letters A. 1998;**81**:3856

[29] Yomba E, Kofane TC. Solutions of the lowest order complex Ginzburg-Landau equation. Journal of the Physical Society of Japan. 2000;**69**:1027

[30] Gonpe Tafo JB, Nana L, Kofane TC. Effects of nonlinear gradient terms on the defect turbulence regime in weakly dissipative systems. Physical Review E. 2017;**96**:022205

[31] Bottin S, Lega J. Pulses of tunable size near a subcritical bifurcation. European Physical Journal B. 1998;**5**:299

[32] Thual O, Fauve S. Localized structures generated by subcritical instabilities. Journal of Physiology, Paris. 1988;**49**:1829

[33] Chaté H. Spatiotemporal intermittency regimes of the one-dimensional complex Ginzburg-Landau equation. Nonlinearity. 1994;**7**:185

[34] Newell AC, Nazarenko S, Biven L. Wave turbulence and intermittency. Physica D: Nonlinear Phenomena. 2001; **152**:550

[35] Lvov YV, Tabak EG. Hamiltonian formalism and the Garrett-Munk spectrum of internal waves in the ocean. Physical Review Letters. 2001;**87**:168501

[36] Coullet P, Elphick C, Repaux D. Nature of spatial chaos. Physical Review Letters. 1987;**58**:431

[37] Tobias SM, Knobloch E. Breakup of spiral waves into chemical turbulence. Physical Review Letters. 1998;**80**:4811

[38] Aranson IS, Aranson L, Kramer L, Weber A. Stability limits of spirals and traveling waves in nonequilibrium media. Physical Review A. 1992;**46**: R2992

[39] Voss HU, Kolodner P, Abel M, Kurths J. Amplitude equations from spatiotemporal binary-fluid convection data. Physical Review Letters. 1999;**83**: 3422

[40] Bot P, Mutabazi I. Dynamics of spatio-temporal defects in the Taylor-Dean system. European Physical Journal B. 2000;**13**:141

[41] Beta C, Bertram M, Mikhailov AS, Rotermund HH, Ertl G. Controlling turbulence in a surface chemical reaction by time-delay autosynchronization. Physical Review E. 2003;**67**:046224

[42] Beta C, Mikhailov AS. Controlling spatiotemporal chaos in oscillatory reaction-diffusion systems by time delay auto synchronization. Physica D: Nonlinear Phenomena. 2004;**199**:173

[43] Falcke M, Engel H, Neufeld M. Cluster formation, standing waves, and stripe patterns in oscillatory active media with local and global coupling. Physical Review E. 1995;**52**:763

[44] Falcke M, Engel H. Pattern formation during the CO oxidation on Pt(110) surfaces under global coupling. The Journal of Chemical Physics. 1994; **101**:6255

[45] Duan J, Holmes P. On the Cauchy problem of a generalized Ginzburg-Landau equation. Nonlinear Analysis. 1994;**22**:1033

[46] Barten W, Lücke M, Kamps M, Schmitz R. Convection in binary fluid mixtures. II. Localized traveling waves. Physical Review E. 1995;**51**:5662

[47] Lücke M, Barten W, Kamps M. Convection in binary mixtures: The role of the concentration field. Physica D: Nonlinear Phenomena (Amsterdam, Netherlands). 1992;**61**:183

[48] Akhmediev N, Soto-Crespo JM. Strongly asymmetric soliton explosions. Physical Review E. 2004;**70**:036613

[49] Burke J, Knobloch E. Homoclinic snaking: Structure and stability. Chaos. 2007;**17**:037102

[50] Sherratt JA, Smith MJ. Transition to spatiotemporal chaos via stationary branching shocks and holes. Physica D: Nonlinear Phenomena (Amsterdam, Netherlands). 2012;**241**:1671

[51] Urzagasti D, Laroze D, Pleiner H. Localized chaotic patterns in weakly dissipative systems. The European Physical Journal Special Topics. 2014; **223**:141